Label-free tetra-modal molecular imaging of living cells with CARS, SHG, THG and TSFG (coherent anti-Stokes Raman scattering, second harmonic generation, third harmonic generation and third-order sum frequency generation)

Hiroki Segawa,[1] Masanari Okuno,[1] Hideaki Kano,[1,5] Philippe Leproux,[2,3] Vincent Couderc,[2] and Hiro-o Hamaguchi[1,4,*]

[1]*Department of Chemistry, School of Science, The University of Tokyo, Hongo, 7-3-1, Bunkyo, Tokyo,113-0033, Japan*

[2]*Institut de Recherche XLIM, UMR CNRS 6172, 123 Avenue Albert Thomas, 87060 Limoges Cedex, France*

[3]*LEUKOS, ESTER Technopole, 1 Avenue d'Ester, 87069 Limoges Cedex, France*

[4]*Institute of Molecular Science and Department of Applied Chemistry, National Chiao Tung University, Ta Hsueh Road 1001, Hsinchu 300, Taiwan*

[5]*Currently with the Division of Applied Physics, Faculty of Pure and Applied Sciences, University of Tsukuba, 1-1-1, Tennodai, Tsukuba, Ibaraki 305-8577, Japan*

[*]*hhama@chem.s.u-tokyo.ac.jp*

Abstract: We have developed a new multimodal molecular imaging system that combines CARS (coherent anti-Stokes Raman scattering), SHG (second harmonic generation), THG (third harmonic generation) and multiplex TSFG (third-order sum frequency generation) using a subnanosecond white-light laser source. Molecular composition and their distribution in living cells are clearly visualized with different contrast enhancements through different mechanisms of CARS, SHG, THG and TSFG. A correlation image of CARS and TSF reveals that the TSF signal is generated predominantly from lipid droplets inside a cell as well as the peripheral cell wall.

OCIS codes: (180.4315) Nonlinear microscopy; (180.5655) Raman microscopy; (300.6230) Spectroscopy, coherent anti-Stokes Raman scattering; (190.4180) Multiphoton processes.

References and links

1. E. J. Gualda, G. Filippidis, G. Voglis, M. Mari, C. Fotakis, and N. Tavernarakis, "*In vivo* imaging of cellular structures in *Caenorhabditis elegans* by combined TPEF, SHG and THG microscopy," J. Microsc. **229**(1), 141–150 (2008).
2. J. Sun, T. Shilagard, B. Bell, M. Motamedi, and G. Vargas, "In vivo multimodal nonlinear optical imaging of mucosal tissue," Opt. Express **12**(11), 2478–2486 (2004).
3. W. R. Zipfel, R. M. Williams, R. Christie, A. Y. Nikitin, B. T. Hyman, and W. W. Webb, "Live tissue intrinsic emission microscopy using multiphoton-excited native fluorescence and second harmonic generation," Proc. Natl. Acad. Sci. U.S.A. **100**(12), 7075–7080 (2003).
4. H. Chen, H. Wang, M. N. Slipchenko, Y. Jung, Y. Shi, J. Zhu, K. K. Buhman, and J. X. Cheng, "A multimodal platform for nonlinear optical microscopy and microspectroscopy," Opt. Express **17**(3), 1282–1290 (2009).
5. J. W. Jhan, W. T. Chang, H. C. Chen, M. F. Wu, Y. T. Lee, C. H. Chen, and I. Liau, "Integrated multiple multi-photon imaging and Raman spectroscopy for characterizing structure-constituent correlation of tissues," Opt. Express **16**(21), 16431–16441 (2008).
6. C. P. Pfeffer, B. R. Olsen, F. Ganikhanov, and F. Légaré, "Multimodal nonlinear optical imaging of collagen arrays," J. Struct. Biol. **164**(1), 140–145 (2008).
7. D. Yelin and Y. Silberberg, "Laser scanning third-harmonic-generation microscopy in biology," Opt. Express **5**(8), 169–175 (1999).
8. S. Yue, M. N. Slipchenko, and J. X. Cheng, "Multimodal nonlinear optical microscopy," Laser Photon. Rev. **5**(4), 496–512 (2011).
9. A. Zoumi, A. Yeh, and B. J. Tromberg, "Imaging cells and extracellular matrix *in vivo* by using second-harmonic generation and two-photon excited fluorescence," Proc. Natl. Acad. Sci. U.S.A. **99**(17), 11014–11019 (2002).

#162203 - $15.00 USD Received 30 Jan 2012; revised 24 Mar 2012; accepted 28 Mar 2012; published 11 Apr 2012

10. H. Kano and H. O. Hamaguchi, "Supercontinuum dynamically visualizes a dividing single cell," Anal. Chem. **79**(23), 8967–8973 (2007).
11. M. Okuno, H. Kano, P. Leproux, V. Couderc, and H. O. Hamaguchi, "Ultrabroadband multiplex CARS microspectroscopy and imaging using a subnanosecond supercontinuum light source in the deep near infrared," Opt. Lett. **33**(9), 923–925 (2008).
12. N. Ji, K. Zhang, H. Yang, and Y. R. Shen, "Three-dimensional chiral imaging by sum-frequency generation," J. Am. Chem. Soc. **128**(11), 3482–3483 (2006).
13. M. Okuno, H. Kano, P. Leproux, V. Couderc, J. P. R. Day, M. Bonn, and H. O. Hamaguchi, "Quantitative CARS molecular fingerprinting of single living cells with the use of the maximum entropy method," Angew. Chem. Int. Ed. Engl. **49**(38), 6773–6777 (2010).
14. H. J. van Manen, Y. M. Kraan, D. Roos, and C. Otto, "Intracellular chemical imaging of heme-containing enzymes involved in innate immunity using resonance Raman microscopy," J. Phys. Chem. B **108**(48), 18762–18771 (2004).
15. Y. S. Huang, T. Karashima, M. Yamamoto, and H. O. Hamaguchi, "Molecular-level investigation of the structure, transformation, and bioactivity of single living fission yeast cells by time- and space-resolved Raman spectroscopy," Biochemistry **44**(30), 10009–10019 (2005).
16. J. X. Cheng and X. S. Xie, "Green's function formulation for third-harmonic generation microscopy," J. Opt. Soc. Am. B **19**(7), 1604–1610 (2002).
17. S. Feng and H. G. Winful, "Physical origin of the Gouy phase shift," Opt. Lett. **26**(8), 485–487 (2001).
18. P. J. Campagnola, A. C. Millard, M. Terasaki, P. E. Hoppe, C. J. Malone, and W. A. Mohler, "Three-dimensional high-resolution second-harmonic generation imaging of endogenous structural proteins in biological tissues," Biophys. J. **82**(1), 493–508 (2002).
19. B. Byers and L. Goetsch, "Behavior of spindles and spindle plaques in the cell cycle and conjugation of *Saccharomyces cerevisiae*," J. Bacteriol. **124**(1), 511–523 (1975).
20. S. L. Jaspersen and M. Winey, "The budding yeast spindle pole body: structure, duplication, and function," Annu. Rev. Cell Dev. Biol. **20**(1), 1–28 (2004).
21. D. Débarre, W. Supatto, A. M. Pena, A. Fabre, T. Tordjmann, L. Combettes, M. C. Schanne-Klein, and E. Beaurepaire, "Imaging lipid bodies in cells and tissues using third-harmonic generation microscopy," Nat. Methods **3**(1), 47–53 (2006).
22. V. Barzda, C. Greenhalgh, J. Aus der Au, S. Elmore, J. van Beek, and J. Squier, "Visualization of mitochondria in cardiomyocytes by simultaneous harmonic generation and fluorescence microscopy," Opt. Express **13**(20), 8263–8276 (2005).

1. Introduction

Multimodal nonlinear optical imaging is now widely used to become one of the most powerful methods to analyze biological systems such as living cells and tissues [1–6]. Using various nonlinear optical processes, we can visualize the molecular compositions and their distribution in living cells with different contrast enhancements. One of the typical multimodal imaging techniques is the combination of two-photon excitation fluorescence (TPEF) with second harmonic generation (SHG) or third harmonic generation (THG) [1–3]. While TPEF visualizes labeled or intrinsic fluorophores, SH and TH complementarily probe non-labeled objects in cells and tissues. SH is sensitive to a non-centrosymmetric structure such as collagen fibers in a tissue and TH is sensitive to an interface where optical properties change [7]. Recently, multimodal nonlinear optical imaging has been applied to cancer diagnosis [8].

A Ti:Sapphire laser oscillator is often employed for multimodal nonlinear optical imaging in order to obtain high photon density at the focal position [2–4,6]. With such a light source, however, we have to tune the laser wavelength to achieve resonances [6,9]. This difficulty is bypassed with the use of the recently developed supercontinuum (or white-light laser source), since its broad spectral profile, typically spanning more than an octave, automatically fulfills multiple resonance conditions. Many resonances can thus be detected simultaneously in the form of a spectrum and full spectral information on molecules in a living cell is obtainable together with their detailed spatial distributions (spectral imaging) [10,11].

In the present study, we attempt tetra-modal molecular imaging using multiplex coherent anti-Stokes Raman scattering (CARS), SHG, THG and multiplex third-order sum frequency generation (TSFG). TSFG is a third order nonlinear optical process similar to THG. The TH signal is generated by single color excitation with an angular frequency of ω_1 as $\omega_{TH} = \omega_1 + \omega_1 + \omega_1$. On the other hand, the TSFG process is expressed as $\omega_{TSF} = \omega_1 + \omega_2 + \omega_3$ (see Fig. 1(a) and 1(b)). Although second-order sum frequency generation microscopy is reported [12], no report has been made on TSFG microscopy. In the present experimental condition,

#162203 - $15.00 USD Received 30 Jan 2012; revised 24 Mar 2012; accepted 28 Mar 2012; published 11 Apr 2012

the TSF signal is generated from the combination of a narrow-band laser (ω_1) and a broad-band white-light laser (ω_2), with $\omega_{TSF} = 2\omega_1 + \omega_2$ and $\omega_1 + 2\omega_2$. Using this new multimodal imaging scheme, living cells are clearly visualized with different molecular contrasts through multiplex CARS, SHG, THG and multiplex TSFG simultaneously.

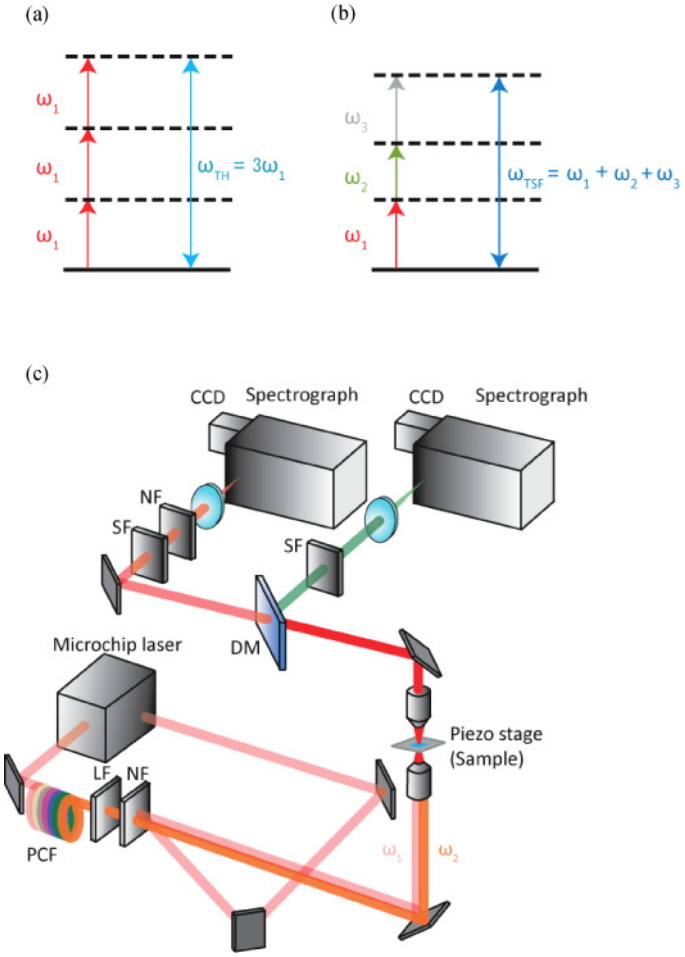

Fig. 1. Diagrams of (a) the THG process, (b) the TSFG process and (c) the experimental setup for multiplex CARS, SHG, THG and multiplex TSFG multimodal imaging. PCF stands for photonic crystal fiber, SF short-pass filter, LF long-pass filter, NF notch filter, and DM dichroic mirror.

2. Experimental

The experimental setup used in the present study is schematically shown in Fig. 1(c). We use a Q-switched subnanosecond microchip Nd:YAG laser as the primary laser source. The fundamental output (1064 nm, 33 kHz) is equally divided by a beam splitter. One portion is used as the ω_1 beam and the other is coupled into a photonic crystal fiber (PCF). The white-light continuum from the PCF (1.1 μm to 1.6 μm) is used as the ω_2 radiation. The broadband ω_2 beam passes through long-pass filters in order to eliminate the spectral component from 350 nm to 1064 nm. The ω_1 and ω_2 beams are superposed by a notch filter, which reflects only 1064-nm ω_1 beam and transmits the other spectral components (ω_2 beam), and then introduced into a modified inverted microscope (Nikon: ECLIPSE Ti). The ω_1 and ω_2 beams are tightly focused onto the sample by an objective (Nikon: Plan 100x / NA 1.25), and forward-propagating signals are collected by another objective (Nikon: Plan S Fluor 40x / NA

#162203 - $15.00 USD Received 30 Jan 2012; revised 24 Mar 2012; accepted 28 Mar 2012; published 11 Apr 2012

0.9). The sample is placed on a piezo stage (Mad City Lab: Nano-LP200), and is scanned in lateral direction in order to obtain spectra and images without moving the focal spots of the two laser beams. The signal beam is then divided by a dichroic mirror into the visible and near-infrared (NIR) spectral components, and they are detected separately by two sets of spectrometers and detectors. After eliminating the remnant of excitation laser beams by a short-pass (< 1050 nm) filter and a 1064-nm notch filter, we use a NIR-sensitive polychromator (Princeton Instruments: LS785) and a CCD camera (Princeton Instruments: PIXIS 100BR eXcelon) for the CARS signal detection in the NIR region. The CARS spectral coverage is over 3000 cm^{-1}, so that we can measure both the fingerprint region and the X-H (C-H, N-H, and O-H) stretch region simultaneously. Visible spectral components containing SH, TH, and the multiplex TSF signals pass a short-pass (< 800 nm) filter for blocking the laser light, and are detected by another spectrometer (Princeton Instruments: SpectraPro 300i) and a CCD camera (Princeton Instruments: PIXIS 100BR eXcelon). Since two CCD cameras and the piezo stage are electronically synchronized, we can perform multiplex CARS, SHG, THG and multiplex TSFG spectral imaging simultaneously.

The sample was living budding yeast cell (a zygote of *Saccharomyces cerevisiae* and *Saccharomyces bayanus*) cultured in the YPD medium (a yeast complete medium containing yeast extract, glucose and polypeptone) except for those shown in the left side image of Figs. 3(a) and 3(b), which were cultured in the LA (lactic acid) medium. Before the measurement, yeast cells were sandwiched by two cover slips, and were sealed with Vaseline to prevent volatilization of the medium. Yeast cells were immobilized physically by a small sample volume between the two cover slips. The sample thickness was thus close to the diameter of budding yeast cells.

3. Results and discussion

Figure 2(a) shows the spectral profiles of the obtained signals in the visible region (300 nm-600 nm) and in the NIR region (880 nm-980 nm). The blue and the orange spectra have been obtained from the two different positions in the same living yeast cell marked with blue and orange crosses in Fig. 2(b). In the visible region, two sharp peaks are observed at 532 nm and 355 nm. They are assigned to the SH and TH of the ω_1 radiation (1064 nm). Since the spectral profile is not intensity-corrected, the TH signal apparently looks weak because of the low transmittance of the microscope objective, the low throughput of the polychromator, and the low sensitivity of the CCD camera. Besides the SH and TH signals, a broad spectral feature is observed around 390 nm. This signal is ascribed to the multiplex TSFG processes ($2\omega_1 + \omega_2$ and $\omega_1 + 2\omega_2$). The possible wavelength of TSF under the present experimental condition is calculated as 359-457 nm. This is consistent with the experimentally obtained spectrum shown in Fig. 2(a). The intensity is decreased at the longer wavelength region (> 390 nm), probably because the number of the possible combination of the ω_2 spectral components decreases. In the present study, no SFG ($\omega_1 + \omega_2$) has been found most probably due to the low power density of each spectral component of the white-light continuum and the requisition of non-centrosymmetric structure. In addition to this, we also observe CARS spectra simultaneously with SH, TH and TSF. Using the maximum entropy method, we retrieve the $\mathrm{Im}[\chi^{(3)}]$ spectra from the observed CARS spectral profiles, which are often interfered by the nonresonant background [13]. The spectra shown for the 880-980 nm region (Fig. 2(a)) are the retrieved $\mathrm{Im}[\chi^{(3)}]$ spectra after noise reduction with a singular value decomposition analysis [14]. According to our previous study [15], the spectra shown in Fig. 2(a) correspond to a lipid-rich part (blue) and a protein-rich part (orange) in a living budding yeast cell. Because the SH, TH, TSF signals and CARS signals are obtained with their spectral information at each spatial points, we are able to obtain various images simultaneously with different contrast enhancement mechanisms. Figure 2 shows (b) the optical image, (c) the SH image, (d) the TH image, (e) the TSF image, (f) the CARS image at 1440 cm^{-1} (CH_2 bend mode of lipids) and (g) the CARS image at 1003 cm^{-1} (phenylalanine residue of proteins). Using the present experimental setup, label-free tetra-modal molecular imaging of multiplex CARS, SHG, THG and multiplex TSFG has been achieved. To the best

#162203 - $15.00 USD Received 30 Jan 2012; revised 24 Mar 2012; accepted 28 Mar 2012; published 11 Apr 2012

of our knowledge, this is the first report that multiplex TSFG is used for the imaging of living cells.

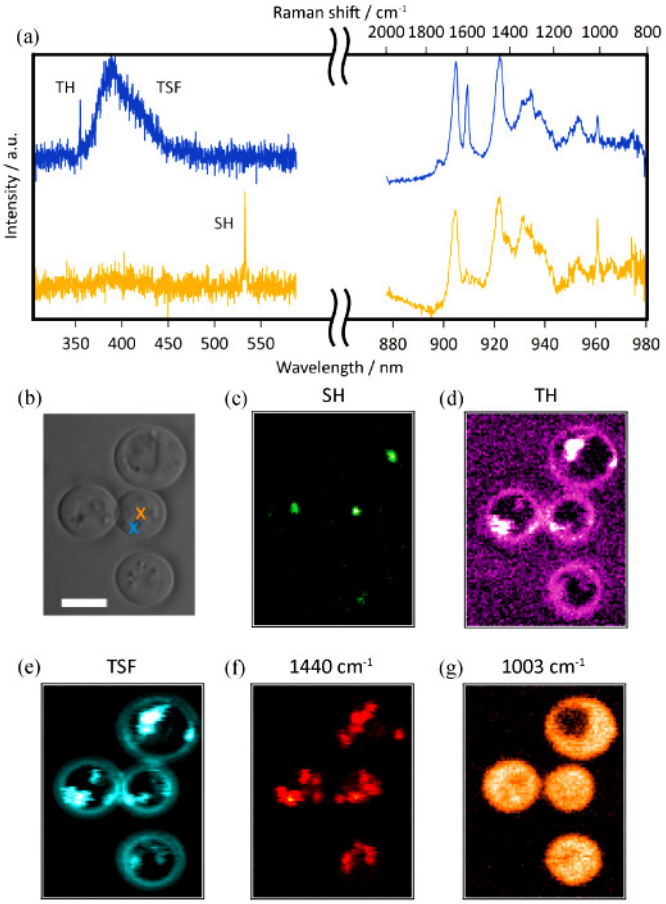

Fig. 2. (a) Spectral profiles of the visible region and the NIR region; the others are the images of yeast cells corresponding to (b) optical; (c) SH; (d) TH; (e) TSF; (f) 1440 cm^{-1}(CH_2 bend mode) ; (g) 1003 cm^{-1}(phenylalanine residue) image. The white bar in (b) corresponds to 5 μm. Blue and orange crosses are the position where each spectrum was obtained.

The TH image in Fig. 2(d) is very similar to the TSF image in Fig. 2(e). It is known that, under a tightly focused condition, the TH signal is selectively generated at an interface [7,16]. This selectivity arises from the Gouy phase shift [17] under a tightly focused condition that shortens the coherence length of the THG process. Thus, the TH signal vanishes for an isotropic material but becomes detectable for a system with optical inhomogeneity such as interfaces [7,16]. Since the TSFG process is described by the same framework with the THG process, it is not surprising if the TSF image is similar to the TH image. However, for multimodal imaging with CARS, there is a notable difference between THG and TSFG. The TSFG and CARS processes require both the ω_1 and ω_2 radiations. In contrast, the THG process requires only the ω_1 radiation. Therefore, the CARS and TSF signals originate from the same position where the ω_1 and ω_2 radiations are spatially overlapped, while the CARS and TH signals do not. This is an advantage of CARS and TSFG simultaneous imaging. Moreover, the wavelengths of TH and TSF signals correspond to 355 nm and 359-457 nm, respectively. Therefore, we can also investigate the electronic resonance effect in the broad spectral range by simultaneous detection of TH and TSF.

#162203 - $15.00 USD Received 30 Jan 2012; revised 24 Mar 2012; accepted 28 Mar 2012; published 11 Apr 2012

Now we discuss the origins of the SH and TSF signals with reference to the CARS. Figure 3(a) shows the optical images of budding yeast cells and the corresponding SH images are given in Fig. 3(b). Figure 3(c) shows the averaged Im[$\chi^{(3)}$] spectrum at the SH bright spots in 4 cells on the right side image in Figs. 3(a) and 3(b). Compared with our previous study [15], this spectrum is much similar to the typical protein-rich spectrum in the yeast cell. Hence the organelle giving the SH signal is mainly composed of proteins. According to a previous study of SH imaging of nematode [18], centrosomes and microfibers are SH active. In the case of budding yeast, centrosome does not exist but a similar organelle, spindle pole body (SPB) does exist. Functions of SPB are known to be similar to those of centrosomes in animal cells [19]. Since the SPB is composed of filamentous proteins [20] as centrosome is, we consider that SH visualize SPB in the present experimental condition.

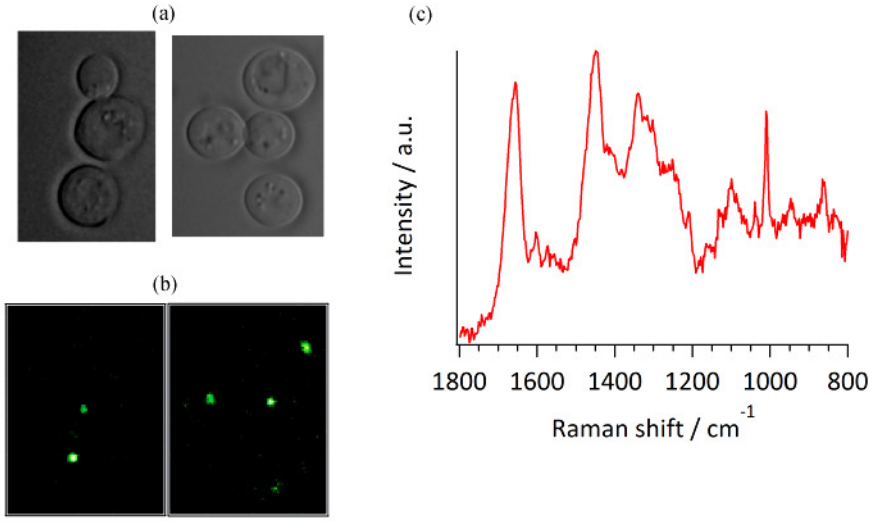

Fig. 3. (a) Optical image, (b) corresponding SH image. On the left side image, two cells have a bright spot and one cell (upper one) do not. On the right side image, all cell have a bright spot. (c) The averaged Im[$\chi^{(3)}$] spectrum at the 4 SH bright spots indicated in the right side image of (b).

Next we discuss the origin of TSF. A lipid body is known to give a strong TH signal due to its large difference of the refractive index and $\chi^{(3)}$ between lipids and cytosol [21]. Taking into account the fact that a lipid molecule has a large Raman cross section for the CH_2 bend mode, both TSF and CARS CH_2 bend images should visualize mainly lipid droplets inside yeast cells. The correlation image of TSF image (Fig. 4(a)) and CH_2 bend mode image (Fig. 4(b)) is shown in Fig. 4(c), calculated by the following equation [22],

$$C_{ij} = \frac{\dfrac{a_{ij}}{\left(a_{ij}\right)_{Max}} \cdot \dfrac{b_{ij}}{\left(b_{ij}\right)_{Max}}}{\left(\dfrac{a_{ij}}{\left(a_{ij}\right)_{Max}} \cdot \dfrac{b_{ij}}{\left(b_{ij}\right)_{Max}} \right)_{Max}},$$

where a_{ij} and b_{ij} correspond to the signal intensities of the TSF and the CH_2 bend CARS at the (i, j) pixel. The value of C_{ij} represents the intensity correlation at the (i, j) pixel between the two images. The correlation image shows high correlation inside the cell. Therefore, by the combination of TSF and CARS, we can conclude that these image contrasts are generated from lipid droplets.

#162203 - $15.00 USD Received 30 Jan 2012; revised 24 Mar 2012; accepted 28 Mar 2012; published 11 Apr 2012

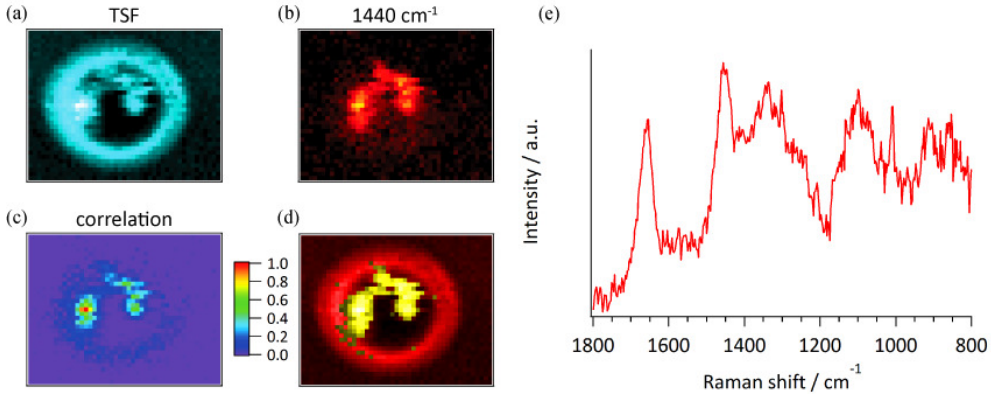

Fig. 4. (a) TSF image; (b) CARS image at 1440 cm^{-1} (CH_2 bend); (c) correlation image between (a) and (b); (d) high correlation area (yellow) and low correlation area (red) of TSF image (a); (e) The integrated spectrum over the peripheral red area of (d).

Moreover, we can simultaneously obtain information on the low correlation region of CARS and TSF. Figure 4(d) shows the decomposed TSF image based on the correlation value (high correlation region corresponds to yellow and low correlation region corresponds to red). The averaged $\mathrm{Im}[\chi^{(3)}]$ spectrum over the red region is shown in (e). According to our previous study, this spectral profile is ascribed to the polysaccharide such as mannan and β-1,3-glucan [15]. The red region in Fig. 4(d) therefore corresponds to the cell wall, visualized by the optical interface between the cell and the surrounding medium.

4. Conclusion

We have developed a label-free tetra-modal molecular imaging system. The multiplex CARS, SHG, THG and multiplex TSFG signals are obtained simultaneously using a white-light laser source. This technique is applied to budding yeast cells. By the combination of SH-CARS and TSF-CARS, we visualized intracellular organelles such as SPB, lipid droplets and cell wall with their molecular information.

Acknowledgment

The authors gratefully acknowledge J. Ukon, HORIBA, Ltd. for assisting a fruitful collaboration between Japanese and French labs. This work is supported by a SENTAN-S from JST. H. Kano gratefully acknowledges financial support by Grand-Aid for Scientific Research on Priority Areas “Molecular Science for Supra Functional Systems” [477] from MEXT, and the Global COE Program for “Chemistry Innovation”. The authors thank LEUKOS Company for technical support with the dual-output supercontinuum laser source. The authors thank Suntory for supplying us the yeast cells.

#162203 - $15.00 USD Received 30 Jan 2012; revised 24 Mar 2012; accepted 28 Mar 2012; published 11 Apr 2012